Available online at www.sciencedirect.com
ScienceDirect
Ceramics International 34 (2008) 141–149
CERAMICS INTERNATIONAL
www.elsevier.com/locate/ceramint

Nanostructured Nd:YAG powders via gel combustion: The influence of citrate-to-nitrate ratio

Jiang Li [a,b], Yubai Pan [a,*], Fagui Qiu [a,b], Yusong Wu [a,b], Jingkun Guo [a]

[a] State Key Lab of High Performance Ceramics and Superfine Microstructure, Shanghai Institute of Ceramics, Chinese Academy of Sciences, Shanghai 200050, PR China
[b] Graduate School of the Chinese Academy of Sciences, Beijing 100039, PR China

Received 22 July 2006; received in revised form 19 August 2006; accepted 22 September 2006
Available online 7 November 2006

Abstract

Nanostructured neodymium doped yttrium aluminum garnet (Nd:YAG) powders were synthesized at low temperature by a gel combustion method with citric acid as fuel and nitrate as oxidizer. The method involves exothermic decomposition of an aqueous citrate–nitrate gel. The decomposition is based on a thermally induced anionic redox reaction. A variety of 1.0 at% Nd:YAG powders with different agglomerate structures were obtained by altering the citrate-to-nitrate ratio γ. The gel with $\gamma = 0.277$ yielded nanocrystalline Nd:YAG at 800 °C without the formation of any intermediate phase. For other gels nanostructured Nd:YAG powders were obtained at 850 °C. The gel with $\gamma = 0.1$ yielded nanostructured Nd:YAG powder with an average particle size of ~40 nm. The stoichiometric citrate-to-nitrate ratio ($\gamma = 0.277$) gave the lowest amount of agglomeration. The decomposition of the gel was investigated by TG–DSC and FTIR. The produced ashes and calcined powders were characterized by XRD, BET and FETEM analysis.

Keywords: Nanostructured Nd:YAG; Gel combustion synthesis; Citrate-to-nitrate ratio

1. Introduction

Recently, polycrystalline Nd:YAG ceramic laser materials have received much attention because the optical quality has been improved greatly and highly efficient laser oscillations could be obtained that comparable in efficiency with Nd:YAG crystals [1–8]. Owing to such application potential of Nd:YAG ceramics, some methods for the synthesis of pure and homogeneous YAG or Nd:YAG powders have been adopted. YAG powders are traditionally produced by a solid-state reaction [9] between the component oxides, which requires tedious mechanical mixing and extensive heat treatment at high temperature to eliminate intermediate phases. The process generally introduces additional impurities and has poor control of particle size. Because of good mixing of the starting materials and excellent chemical homogeneity of the final product, various wet-chemical routes have been proposed to lower the synthesis temperature and eliminate the presence of intermediate phases. These methods include sol–gel [10–13], precipitation [14–16], hydrothermal treatment [17–19], spray pyrolysis [20,21], combustion [22,23] and polymerized complex method [24]. Most of these methods suffer from complexity and time consuming procedures and/or mismatch in the solution behavior of the constituents. For the case of precipitation method, simple solution mixing of the components does not guarantee a precise control of cationic stoichiometry due to the phase separation tendencies of unimetal phases [25]. Also, the difference in the isoelectric points of the constitute species may result in element segregation and non-ideal stoichiometries in the obtained powders. Although the precipitation method has significantly lowered the crystallization temperature, it still requires temperatures in excess of 1000 °C to successfully eliminate other yttrium aluminates and transition alumina. The hydrothermal methods that have resulted in YAG crystallization at lower temperatures are complicated, requiring the use of autoclaves and high pressure for long periods. Products of spray pyrolysis easily result in severe agglomeration, and the

* Corresponding author. Tel.: +86 21 52412820; fax: +86 21 52413903.
E-mail address: ybpan@mail.sic.ac.cn (Y. Pan).

0272-8842/$32.00
doi:10.1016/j.ceramint.2006.09.002

sinterability of the YAG powders is not desirable. The sol–gel methods based on molecular precursors are of predominance compared with other solution routes because they allow chemical interactions among the initial mixture of precursor species favoring the evolution of solid-state structure at atomic level. However, the method suffers from complexity and prolonged reaction time is required.

Gel combustion methods for synthesizing fine powders are of significant interest, primary due to the overall simplicity of the technique. Also the method can guarantee a precise control of cationic stoichiometry and homogeneous mixture of metal ions at the atomic level. Furthermore, the optical properties and laser activity of the Nd:YAG polycrystalline ceramics as a solid-state laser material depend largely on dopants. The homogeneous incorporation of secondary phases in a host poses a challenge to conventional powder milling methods therefore the fabrication of mixed oxide phases by an atomic level approach is of significant interest.

In our previous work [26,27], nanostructured Nd:YAG (YAG) powders were prepared by a simple gel combustion method with citric acid as fuel and nitrate as oxidizers. In this paper, the influences of citrate-to-nitrate ratio on the chemical environment of the gel, thermal behavior, phase transition, crystallite size, surface area, morphology, agglomeration, and the carbonate (free carbon) remaining from the combustion reaction are mainly discussed.

2. Experimental

Nd_2O_3 (Shanghai Yuelong New Materials Co. Ltd., 99.99%) was dissolved in concentrated nitric acid by stirring the mixture at 100 °C for 10 min in a beaker. $Al(NO_3)_3{\cdot}9H_2O$ (Shanghai Zhenxing Chemical Co. Ltd., A.R.) and $Y(NO_3)_3{\cdot}6H_2O$ (Shanghai Yulong New Materials Co. Ltd., A.R.) dissolved in deionized water were added and the resulting mixtures were stirred at 60 °C for 30 min. The molar ratio of Nd:Y was controlled to 1.0% and the mole ratio of (Nd + Y):Al was kept as 3:5. In the mixed-metal nitrate solution, citric acid ($C_6H_8O_7{\cdot}H_2O$, Shanghai Lingfeng Chemical Co. Ltd., A.R.) was added and the citrate-to-nitrate ratio γ (where $\gamma = M_{citrate}/M_{nitrate}$, M = molar amount of the compound) was varied from 0.1 to 0.667 (Table 1). The reason for selecting such a range of γ is based on the concept of propellant [28]. It can be calculated [29] that 0.833 mol of citric acid is required for each mol of nitrate in order to have a stoichiometric redox reaction in the gel that gives $\gamma = 0.277$ (named GS, Table 1). Deficient citric acid in the gel ($\gamma < 0.277$) presents a fuel-lean condition while higher concentrations produce a fuel-rich condition. Such conditions are expected to synthesis nanosized Nd:YAG powders with different properties, as γ alters the extent of redox reaction in the combustion process. In this paper, the word ''gel'' is used for the product of gelling the aqueous solution of nitrate and citric acid by evaporation of water at ~80 °C. The ''ash'' is the combusted product of the gel, whereas ''powder'' refers to the calcined product of the ash. Gel, ash and powder are named G#, A# and P#, respectively [30].

The mixed Y–Al–Nd citrate–nitrate aqueous solution was continuously stirred at 50–60 °C to obtain yellowish solution of the desired component. The solution was concentrated by evaporation at a solution temperature of ~80 °C under constant stirring, producing a transparent gel. A portion of this gel was collected for characterization. Some of the gel was rapidly heated to 200 °C and then combusted in different fashion depending on γ and yielded a fluffy product along with the evolution of a brown fume. The calcinations of all the combusted products were carried out at various temperatures from 500 to 1100 °C in air for 2 h with a heating rate of 5 °C min^{-1}.

TG–DSC analysis was recorded on a Netzsch STA 449C instrument. Measurements were taken under a continuous flow of air (20 ml min^{-1}). Samples were heated at 10 °C min^{-1} to 1200 °C and then cooled to ambient in air.

Phase identification was performed by a Rigaku D/max2200PC X-ray diffractometer (XRD) using nickel filtered Cu Kα radiation (1.5406 Å) in the range of $2\theta = 10–80°$. The tube current and voltage were 40 mA and 40 kV, respectively. The scanning speed was 4° min^{-1} and the step size was 0.02. The crystallite size of the calcined powders was calculated from X-ray peak broadening using Scherrer formula.

Specific surface area analyses were conducted at 77 K using a Norcross ASAP 2010 Micromeritics, with N_2 as the absorbate gas. Samples were degassed at 150 °C until the air pressure was below 5 μmHg. The specific surface areas were calculated using the BET multipoint method with eight data points.

FTIR of the as-prepared and calcined powders were measured on a Nicolet NEXUS 7000C spectrophotometer in the 400–4000 cm^{-1} range using the KBr pellet (~1 wt% sample) method. Each analysis consisted of a minimum of 32 scans and the resolution was ±2 cm^{-1}.

Microstructures were observed on a JEOL JEM 2100F FETEM instrument. Samples were prepared using a carbon-coated copper grid (150 mesh). Powders were dispersed in ethanol using an ultrasonic horn, and then a drop of the

Table 1
Chemical composition of the gels and some of their properties

Gel no.	Nitrate	Citric acid	γ	Gel as observed	Decomposed ash
G1	1	0.3	0.1	Yellowish white	A1 (crumb, grayish brown)
G2	1	0.5	0.167	Yellowish	A2 (crumb, dark brown)
GS	1	0.833	0.277	Yellowish	AS (roast, yellowish)
G3	1	1.0	0.333	Yellowish	A3 (roast, yellowish)
G4	1	2.0	0.667	Yellow	A4 (roast, brown)

dispersed powder/ethanol mixture was deposited on the grid. The grid was then dried in air. The FETEM was used with an accelerating voltage of 200 kV.

3. Results and discussion

3.1. Thermal analysis

For comparison, thermal analyses (TG–DSC) of gels with different citrate-to-nitrate ratios, as well as citric acid were carried out. Fig. 1 shows that in the temperature range of 100–150 °C, endothermic peaks appeared which were attributed to the vaporization of physically absorbed water and the dehydration reaction of gels. It is important to note that these gels, regardless of their citrate-to-nitrate ratios, always showed an exothermal decomposition in their corresponding DSC curves. It has been understood [31,32] that such an exothermic reaction is a result of a thermally induced redox reaction between the two anions present in the gel, where citrate acts as a reductant and nitrate as an oxidant. The decomposition of the gels begins at lower temperatures, as the citrate content in the gel increases. It can be seen from Fig. 1 that the exothermic peak temperature shifts from 230.9 to 204.3 to 173.5 to 171.3 to 162.0 °C for G1, G2, GS, G3 and G4, respectively. Gel G1 decomposed in a single step in TG curve, as shown in Fig. 1(a). However, it did not convert all the citrates into gaseous products, as could be confirmed by the infrared spectra in Fig. 4(a). The 300 °C decomposed ash was contaminated with hydroxycarbonate. Infrared spectra of the ash in Fig. 4(a) show a broad band at 3450 cm^{-1}, two intense bands at 1586 and 1388 cm^{-1} possibly due to ν_{OH}, $\nu_{as}(COO^{-})$ and $\nu_{s}(COO^{-})$ vibrations, respectively, indicate the presence of OH and CO_3

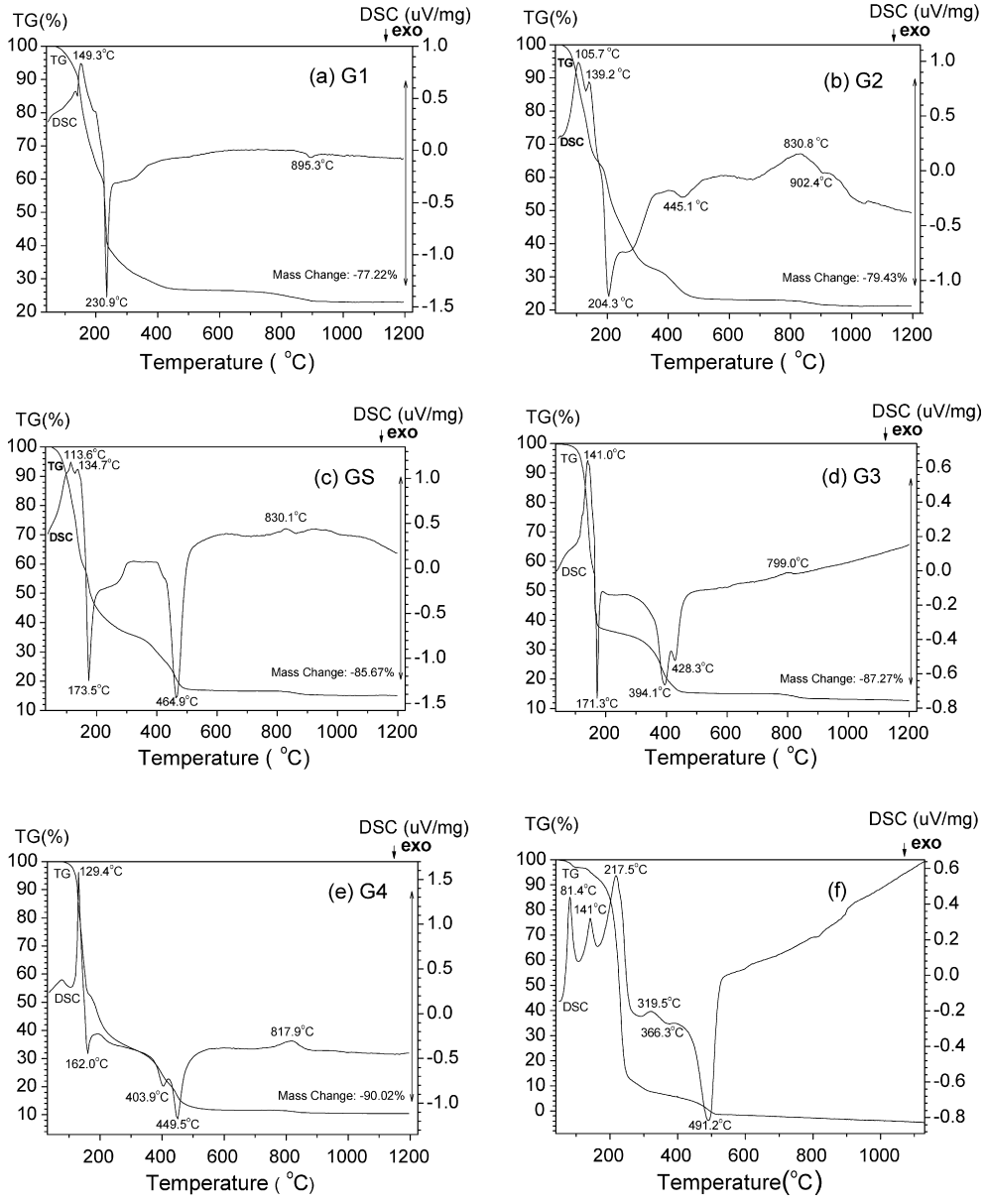

Fig. 1. TG–DSC curves of gels: (a) G1; (b) G2; (c) GS; (d) G3; (e) G4; (f) citric acid.

group. The next tiny mass-loss of G1 in the range of 750–900 °C was due to its carbon or carbonate impurities. Close observation shows that one exothermic peak appears at 895.3 °C, which might result from the crystallization of amorphous Nd:YAG accompanied by the oxidation of carbon present in the amorphous oxide structure [33]. The total mass-loss determined for the production of Nd:YAG from G1 was 77.2%. Calculations of the theoretical mass-loss based on the stoichiometries of the metal nitrate and citric acid in the original solutions yield a value of 83.1% or 74.6% if it is assumed that the water of crystallization of the raw materials is removed during the preparation of the gel. This indicates that a small amount of water remains in the synthesized gel. Gels G2, GS, G3 and G4 show identical decomposition patterns in the TG curves, which occur in two steps in the range of 150–500 °C. Almost negligible mass-losses of the gels associated in the small steps in the TG curves occurred between 800 and 900 °C. The total mass-losses increase with increasing citrate content in the gels. For G2, a distinct endothermic peak and an indistinct exothermic peak appear at 830.8 and 902.4 °C, respectively. We consider that the former might result from the decomposition of carbonate and the later is due to the crystallization of amorphous Nd:YAG accompanied by the oxidation of carbon impurity. GS, G3 and G4 show endothermic peaks in DSC curves at 830.1, 799.0 and 817.9 °C, respectively, which correspond to the decomposition of carbonate. No distinct exothermic peaks resulted from oxidation of carbon or crystallization of amorphous Nd:YAG are detected in these DSC curves. The gel GS with $\gamma = 0.277$ have a theoretically stoichiometric redox reaction. However, it did not stoichiometrically convert all the citrate into gaseous products due to the decomposition of nitrate during the preparation of gel. The decomposed ash (AS) was contaminated with carbon from incomplete combustion of the citrate as well as with hydroxycarbonate, as can be confirmed by the color of AS and the infrared spectrum in Fig. 3(b). When a slightly higher amount of citric acid, relative to stoichiometric composition, was used, a voluminous ash (A3) was produced after combustion of the gel G3 ($\gamma = 0.333$). The TG curve in Fig. 1(d) shows a thermally unstable slope at 171.3 °C, which indicates the formation of an unstable intermediate product that requires further calcinations to yield Nd:YAG. Gel G4 which had an even higher citrate-to-nitrate ratio ($\gamma = 0.667$) showed a similar type of decomposition as G3 in the TG–DSC curve. The combusted product (A4) had a brown color, likely due to contamination by a high amount of unburned carbon. Fig. 1(f) shows the TG–DSC curve of citric acid. It can be seen that citric acid decomposed with a number of endothermic peaks below the temperature of 350 °C. A distinct exothermic peak at 491.2 °C in the corresponding DSC curve indicates the oxidization of free carbon from incomplete combustion of the citric acid.

3.2. Phase analysis by XRD

After the initial heating at 200 °C for 2 h, all the ashes from the gels with different citrate-to-nitrate ratios were amorphous in nature, whether the decomposition occurred in a single step or in two steps. Although the XRD patterns of ashes do not indicate any peak of hydroxycarbonate, hydroxyl and carbonate groups were detected in the corresponding infrared spectra, as shown in Fig. 3(b). Table 2 summarizes the primary phases and colors of powders after heating at temperatures of 500–1100 °C for 2 h in air. When the ashes were calcined below 750 °C for 2 h, all the calcined products were kept amorphous in nature. For the 800 °C calcined products P1, P2, P3 and P4, the characteristic peaks corresponding to the cubic garnet phase appeared with rather weak intensity, as shown in Fig. 2(a). However, the crystallinity of the 800 °C calcined PS appears to be much higher, and all diffraction lines were consistent with the cubic YAG phase (JCPDS No. 82-0575). The phase transition from amorphous to cubic YAG occurred at lower temperature in PS than that observed for others. A previous study [34] shows that the heat evolution is maximum when the citrate-to-nitrate ratio of the gel is slightly more than 0.277. The citrate-to-nitrate ratio of GS was slightly more than the stoichiometric value due to slight decomposition of nitrate. The ashes A1 and A2 with lower citrate concentration gave poorer yields of YAG than did AS at the temperature of 800 °C. The main function of citrate is to provide a polymeric network to hinder cation mobility, which maintains local stoichiometry and minimizes production of undesirable phases. The citrate polymer is also a potential heat source, which will be produced during calcinations. It is possible that the exothermic reaction occurring during heating at 800 °C in the ash (AS) raised the local temperature enough to increase the crystallization kinetics of YAG, compared with A1 and A2, which contain much less citrate to contribute heat. Previous work has found that a high concentration of citric acid [35,36] or an atmosphere that inhibits carbon oxidation [37,38] can retard crystallization of the desired oxide phase from polymeric precursors. In the present work, for all the ashes calcined at temperatures below

Table 2
Phases and colors of powders after 2 h heat treatment in air

Powder	Temperature (°C)				
	500	700	800	850	≥900
P1	Amorphous, dark brown	Amorphous, gray	Amorphous, white	YAG, white	YAG, white
P2	Amorphous, dark brown	Amorphous, dark gray	Amorphous, light gray	YAG, white	YAG, white
PS	Amorphous, dark brown	Amorphous, gray	YAG, white	YAG, white	YAG, white
P3	Amorphous, dark brown	Amorphous, gray	Amorphous, white	YAG, white	YAG, white
P4	Amorphous, dark brown	Amorphous, gray	Amorphous, white	YAG, white	YAG, white

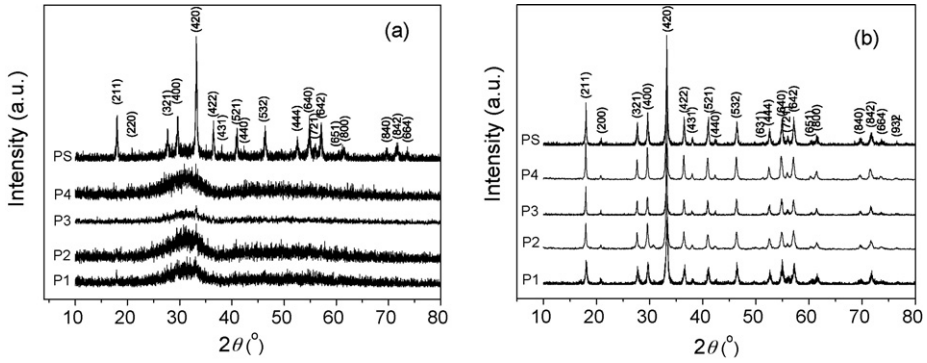

Fig. 2. XRD patterns of powders from ashes calcined at: (a) 800 °C; (b) 850 °C for 2 h.

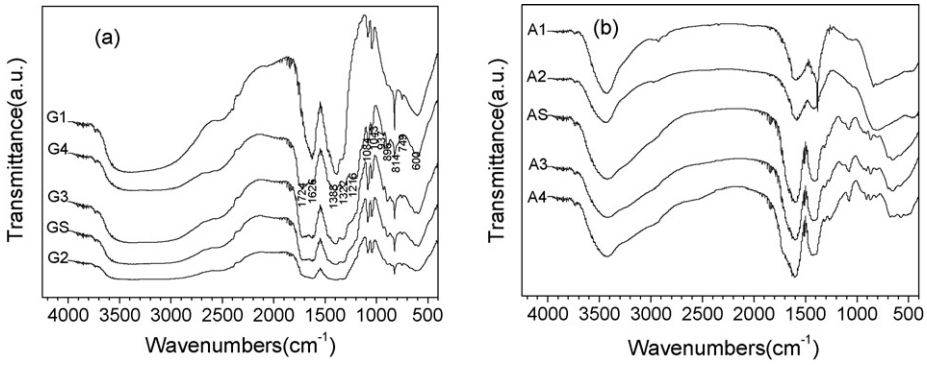

Fig. 3. FTIR spectra of: (a) gels G1, G2, GS, G3, and G4; (b) ashes A1, A2, AS, A3, and A4.

800 °C, the resulting powders were gray in color, indicating hydroxycarbonate decomposition and the presence of carbon. It is likely that at temperatures below 800 °C, for the samples calcined for 2 h, the presence of carbon prevented complete reaction to YAG by increasing diffusion distances of the mixed cations, especially in the higher citrate (the major carbon source) containing ashes A3 and A4. This could explain the greater YAG yield at 800 °C for AS compared with A3 and A4. However, in the DSC curves (Fig. 1) no distinct exothermic peaks are observed between 600 and 900 °C for AS, A3 and A4 due to either YAG crystallization or oxidation of free carbon. Although the XRD patterns of the 800 °C calcined powders do not indicate any peaks of carbonate, the CO_3^{2-} groups were detected in the corresponding infrared spectra shown in Fig. 4.

Fig. 2(b) shows XRD patterns of the 850 °C calcined products P1, P2, PS, P3 and P4 from gels with different citrate-to-nitrate ratios. It is observed that all of the powders had crystallized completely. There was no evidence of any crystalline phase other than YAG, although YAM ($Y_2Al_4O_9$) and YAP ($YAlO_3$) are often present as intermediate phases in the course of synthesis of YAG powder by other wet chemistry methods [39,40]. The high and sharp peaks observed might be associated to the grain growth of the YAG crystallite. However, previous work [41] considered that the formation of YAG was accompanied with a hexagonal YAP (H-YAP) in the gel combustion method. Since YAG is the most stable phase in the Y_2O_3–Al_2O_3 system, the presence of YAP cannot be a result of the decomposition of YAG. Instead, the appearance of YAP may result from chemical inhomogeneity in the precursors [42].

Crystallite size of the 850 °C calcined powders was determined by the X-ray line broadening and calculated using the Scherrer equation:

$$d_{\mathrm{Crys}} = \frac{0.89\lambda}{B\cos\theta}$$

where $B = (B_o^2 - B_c^2)^{1/2}$, B_o is the full width at half maximum (in $2\theta^\circ$), B_c is the correction factor for instrument broadening, θ is the angle of the peak maximum (in $2\theta^\circ$), and λ is the Cu Kα weighted average wavelength. The values of crystallite size calculated from the (4 2 0) XRD peak are shown in Table 3. For P1, P2, PS and P3, the crystallite size increased when γ increased due to the decreased combustion rate of anions. The crystallite size of powder became coarse primarily due to poor heat dissipation by the decomposed gases. But for P4, the crystallite size is smaller than that of P3 because of the lower particle temperature during combustion, which is the dominant factor to affect crystallite size compared with the nature of heat dissipation in the fuel-rich condition.

Table 3
Particle size of powders from ashes calcined at 850 °C for 2 h

Powder no.	P1	P2	PS	P3	P4
S_{ssa} (m^2/g)	35.11	25.97	24.82	16.17	18.66
d_{BET} (nm)	39.7	53.7	56.2	86.3	74.8
d_{Crys} (nm)	30.8	35.2	54.0	59.2	44.3

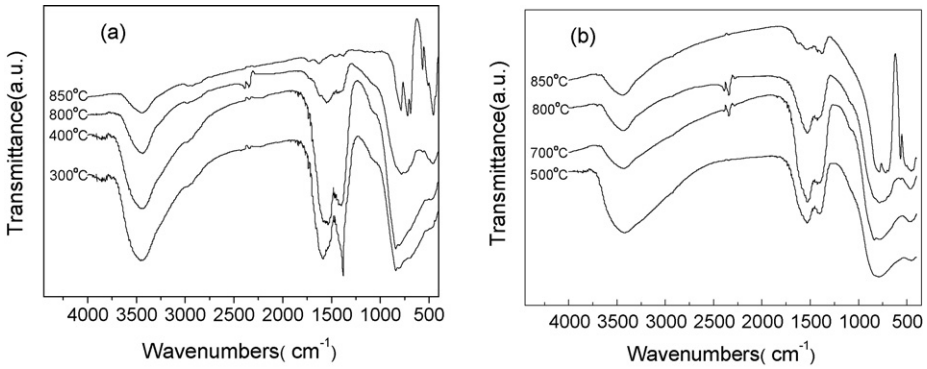

Fig. 4. FTIR spectra of samples from: (a) A1 calcined at 300 °C, 400 °C, 800 °C, and 850 °C; (b) A3 calcined at 500 °C, 700 °C, 800 °C, and 850 °C.

3.3. BET analysis

Table 3 shows that the surface area of the 850 °C calcined powders gradually decreases when citrate-to-nitrate ratio γ goes up to 0.333. The increased crystallite size caused by the nature of heat dissipation is the main factor to affect the specific surface area. Additional, G1 has a complete combustion in a single step. Therefore, a large volume of gases escapes through the ash A1 rapidly. For the gel G1 with lowest citrate-to-nitrate ratio, a minimum amount of fuel yielded a small total reaction enthalpy and superior heat dissipation by the decomposed gases during the rapid combustion. As γ increases, the slow rate of decomposition produces particles with lower surface area. The system has insufficient time to dissipate the heat and thus the local temperature of the particles stays high, which increases the crystallite size. The specific surface area of P4 is slight larger than that of P3 due to relatively small crystallite size, although the scope of agglomeration of P4 is more severe than that of P3. The particle average size is derived from the formula with d_{BET} being the average particle size, ρ the density of the material, and S_{ssa} its specific surface area.

$$d_{\mathrm{BET}} = \frac{6}{\rho S_{\mathrm{ssa}}}$$

Particle size obtained using the above formula is given in Table 3. The change in particle size with γ well accords with the FETEM observations in Fig. 6 and the crystallite size calculated from Scherrer equation. In the case of P1, the particle growth could not get completed owing to the lack of sustainability of the combustion reaction, therefore, counting for smaller particles. In addition, the scope of agglomeration of PS is particularly lower so that individual crystallites showing

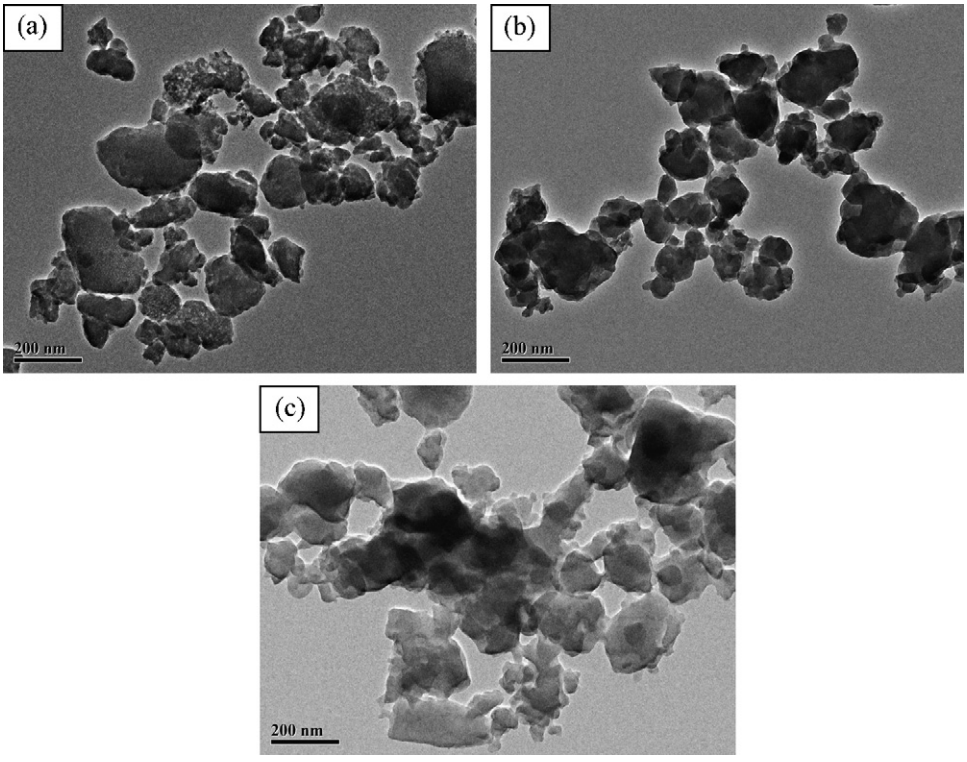

Fig. 5. FETEM micrographs of the ashes: (a) A1; (b) AS; (c) A3.

single-crystal features were observed. For the powder P4 with the highest $\gamma = 0.667$, the agglomeration scope in the corresponding powder is the highest.

3.4. Infrared spectra analyses

An attempt was made to understand the status of anions in the chemical environment of the gel by infrared spectroscopy because the gels differ in their thermal behaviors. As shown in Fig. 3(a), the spectral patterns of G1, G4 differ from G2, GS and G3, with a small shift in some of their band positions as well as with the relative intensities. The spectrum of G1 is dissimilar in the range of 1750–1550 cm^{-1} and that of G4 in the region of 1300–1200 cm^{-1}. The spectra clearly show that the band around 1724 cm^{-1} is not pronounced in G1, compared to the other gels. The particular band is a combination of symmetric stretching and doubly degenerate in-plane bending vibrations of the nitrate (NO_3) group. This confirms the presence of free NO_3 in the gels G2, GS, G3 and G4 and absence of free nitrate in G1. The band around 1216 cm^{-1} in G4 can be attributed to the ν_{CO} stretching vibration of carboxyl (COOH) group, which is not observed in the other gels. It confirms the presence of free citric acid only in G4. The well-resolved band at 1626 cm^{-1} due to $\nu_{N=O}$ vibration indicates the presence of bidentate nitrates in all gels. Other bands of the NO_3 group occur approximately at 1388, 1322, 1043, 814, and 749 cm^{-1} in all gels can be assigned to $\nu(NO_2)$, $\nu(NO_2)$, $\nu(NO)$, $\nu(NO_3)$ and $\nu(NO_3)$ bands, respectively. As to the citrate group, the bands at 1084, 937 and 896 cm^{-1} are possibly due to $\delta(CO)$, $\nu(C–C)$, $\rho_r(CH_2)$ and $\nu(C–C)$ vibrations, respectively. It should be mentioned that the band at 1626 cm^{-1} is possibly overlapped with the $\nu(C=O)$ vibration of the carboxylate group present in the citrate. The spectra indicate citrate coordination to the Y^{3+} in all gels, while the nature of such coordination is not yet clear. A broad absorption band around 3450 cm^{-1} is characteristic band of $\nu(OH)$ for all gels.

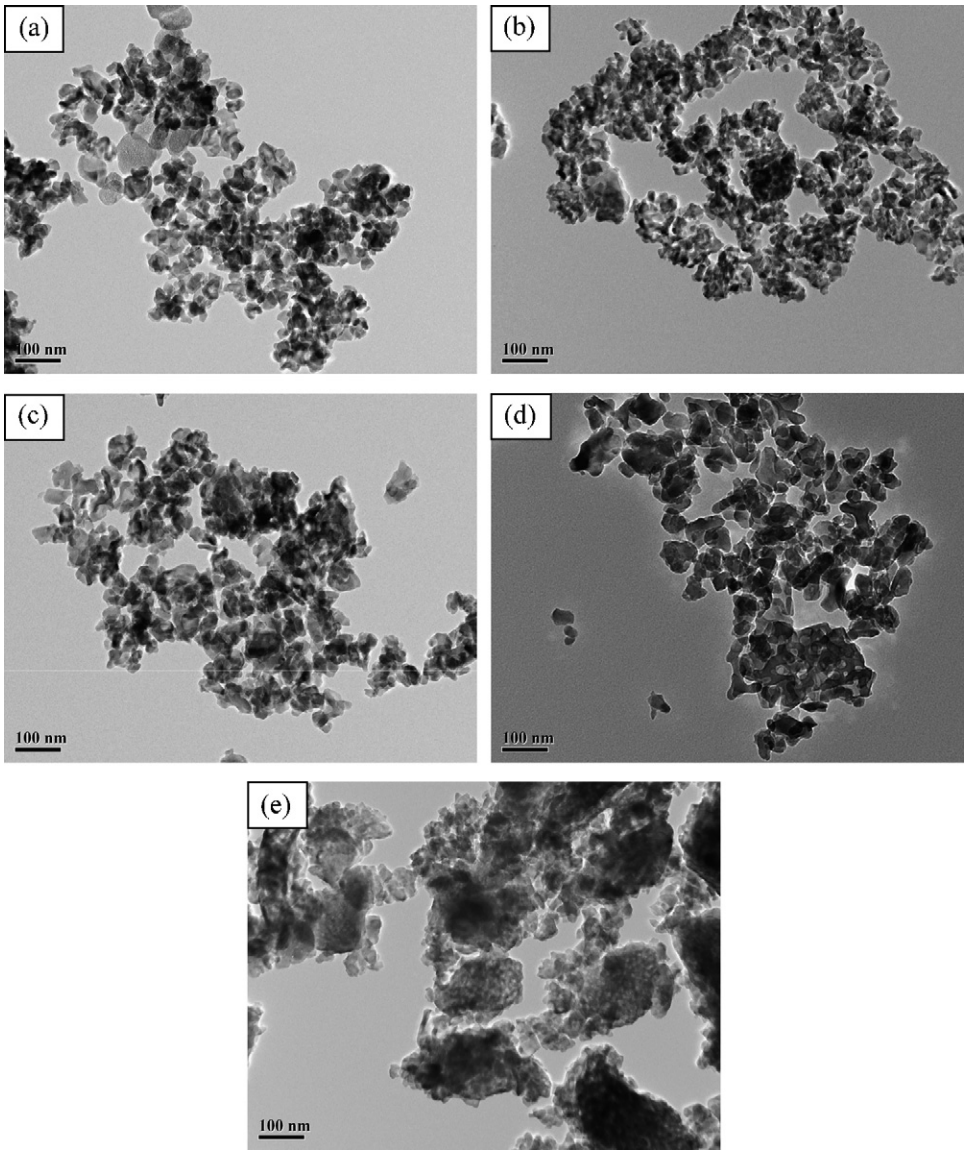

Fig. 6. FETEM micrographs of the 850 °C calcined powders: (a) P1; (b) P2; (c) PS; (d) P3; (e) P4.

Fig. 3(b) shows the FTIR spectra of ashes A1, A2, AS, A3 and A4. The broad peak at 3000–3600 cm^{-1} is a characteristic stretching vibration of ν(OH). Bands localized at 1600 and 1420 cm^{-1} are assigned to asymmetrical and symmetrical stretching vibration of carboxylate, respectively. The spectral patterns of A1, A2 differ from AS, A3 and A4 at 1200–500 cm^{-1}. The difference in spectra is mainly caused by the thermal reactivity.

Fig. 4(a) shows the FTIR spectra of the samples from A1 calcined at different temperatures for 2 h. By 300 °C, two intense bands at 1585 and 1380 cm^{-1} are very close to asymmetrical and symmetrical stretching vibration of carboxylate as mentioned above. There is still a conspicuous OH stretching band around 3450 cm^{-1}. By 400 °C, the spectrum reveals that the carboxylate of the sample transforms into the carbonate with the characteristic asymmetrical split stretching localized at 1530 and 1405 cm^{-1}. The spectrum of the 800 °C sample shows very weak carbonate vibrations. The decomposition of carbonate and crystallization from amorphous YAG phase occur consecutively at this temperature, as can be confirmed by XRD observation in Fig. 2. At 850 °C the carbonate bands have disappeared and been replaced by metal-oxygen vibrations at 790, 720, 690, and 560 cm^{-1}, which corresponds to the formation of crystallite of YAG [43]. Fig. 4(b) shows the FTIR spectra of the samples from A3 calcined at different temperatures for 2 h. It can be seen that carbonate is formed after decomposition of the carboxylate at 500 °C. Carbonate and amorphous YAG phase coexist at the temperature lower than 800 °C. At 850 °C, mono-phase YAG is formed, as indicated in the FTIR patterns.

3.5. FETEM analysis

Fig. 5 shows that the agglomerated structures of selected ashes A1, AS, and A3 change with increase of γ. A combination of flaky and foam agglomerates is visible. The nature of the agglomerates in the ashes indicates that they might have low strength and can be deformed.

Fig. 6 shows the FETEM micrographs of the powders from ashes with different citrate-to-nitrate ratios calcined at 850 °C for 2 h. In a general view, it can be seen that crystallite size increases as γ goes up. The FETEM results confirm the observations of the reaction rates according to the rapid combustion of G1. This then continues to be effective after calcination, giving the powder P1 with smallest particle size. Powders P2, PS, P3 and P4 increase in crystallite size according to the reaction rate that controls the amount of reaction gases formed per time and the amount of heat dissipated. It is considered that in the case of P3 with $\gamma = 0.333$ and P4 with $\gamma = 0.667$, the presence of excess fuel might accelerate the particle agglomeration and result in particles with different morphologies, as shown in Fig. 6(d) and (e), respectively.

4. Conclusions

Nanostructured Nd:YAG powders were synthesized by a simple gel combustion method with citric acid as fuel and nitrate as oxidizer at low temperature. A variety of 1.0 at% Nd:YAG powders with different agglomerate structures can be obtained by altering the citrate-to-nitrate ratio γ. It is found that a higher amount of nitrate in the gel (G1, $\gamma = 0.1$) should be effective in the redox system in completing the combustion of citrate. When a higher amount of citric acid ($\gamma > 0.1$) is used, decomposition occurs in two steps through an unstable intermediate. The gels yield nanostructured Nd:YAG powders at 850 °C without the formation of an intermediate phase. The Nd:YAG powder from the gel with $\gamma = 0.1$ is agglomerated with an average particle size of ~40 nm. Its specific surface area is 35 m^2/g. The stoichiometric citrate-to-nitrate ratio ($\gamma = 0.277$) gives the lowest scope of agglomeration.

Acknowledgements

This work was supported by the Applied Basic Research Programs of Science and Technology Commission Foundation of Shanghai (Grant No. 05DZ22005) and the Key Project of Science and Technology of Shanghai (Grant No. 04DZ14002). We are grateful to Mr. Chundong Wu for the assistance in XRD and FTIR studies. The authors show great appreciation to Dr. Changming Xu and Dr. Lu Gao for helpful discussion.

References

[1] A. Ikesue, I. Furusato, K. Kamata, Fabrication of polycrystallin, transparent YAG ceramics by a solid-state reaction method, J. Am. Ceram. Soc. 78 (1) (1995) 225–228.
[2] A. Ikesue, T. Kinoshita, K. Kamata, K. Yoshida, Fabrication and optical properties of high-performance polycrystalline Nd:YAG ceramics for solid-state lasers, J. Am. Ceram. Soc. 78 (4) (1995) 1033–1040.
[3] A. Ikesue, K. Yoshida, Influence of pore volume on laser performance of Nd:YAG ceramics, J. Mater. Sci. 34 (1999) 1189–1195.
[4] I. Shoji, S. Kurimura, Y. Sato, T. Taira, Optical properties and laser characteristics of high Nd^{3+}-doped $Y_3Al_5O_{12}$ ceramics, Appl. Phys. Lett. 77 (7) (2000) 939–941.
[5] J. Lu, M. Prahu, J. Song, C. Li, J. Xu, K. Ueda, A.A. Kaminskii, H. Yagi, T. Yanagitani, Optical properties and highly efficient laser oscillation of Nd:YAG ceramics, Appl. Phys. B 71 (2000) 469–473.
[6] J. Lu, M. Prahu, J. Xu, K. Ueda, H. Yagi, T. Yanagitani, A.A. Kaminskii, Highly efficient 2% Nd:Yttrium alumina garnet ceramic laser, Appl. Phys. Lett. 77 (23) (2000) 3707–3709.
[7] J. Lu, J. Song, M. Prabhu, J. Xu, K. Ueda, H. Yagi, T. Yanagitani, A. Kudryashov, High-power Nd:$Y_3Al_5O_{12}$ ceramic laser, Jpn. J. Appl. Phys. Lett. 39 (2000) L1048–L1050.
[8] J. Lu, M. Prahu, J. Xu, K. Ueda, H. Yagi, T. Yanagitani, A.A. Kaminskii, Highly efficient Nd:YAG $Y_3Al_5O_{12}$ ceramic laser, Jpn. J. Appl. Phys. Lett. 40 (2001) L552–L554.
[9] D.R. Messier, G.E. Gazza, Synthesis of $MgAl_2O_4$ and $Y_3Al_5O_{12}$ by thermal decomposition of hydrated nitrate mixtures, Am. Ceram. Eng. Sci. 51 (9) (1972) 692–694.
[10] G. Gowda, Synthesis of yttrium aluminates by the sol–gel process, J. Mater. Sci. Lett. 5 (10) (1986) 1029–1032.
[11] R. Manalert, M.N. Rahaman, Sol–gel process and sintering of yttrium aluminum garnet (YAG) powders, J. Mater. Sci. 31 (1996) 3453–3458.
[12] H.M. Wang, M.C. Simmonds, J.M. Rodenburg, Manufacturing of YbAG coatings and crystallisation of the pure and Li_2O-doped Yb_2O_3–Al_2O_3 system by a modified sol–gel method, Mater. Chem. Phys. 77 (2003) 802–807.
[13] H.M. Wang, M.C. Simmonds, Y.Z. Huang, J.M. Rodenburg, Synthesis of nanosize powders and thin films of Yb-doped YAG by sol–gel methods, Chem. Mater. 15 (2003) 3474–3480.

[14] J.W.G.A. Vrolijk, J.W.M.M. Willens, R. Metselaar, Coprecipitation of yttrium and aluminum hydroxide for preparation of yttrium aluminum garnet, J. Eur. Ceram. Soc. 6 (1990) 47–53.
[15] D.J. Sordelet, M. Akinc, M.L. Panchula, Y. Han, M.H. Han, Synthesis of yttrium aluminum garnet precursor powders by homogeneous precipitation, J. Eur. Ceram. Soc. 14 (1994) 123–130.
[16] N. Matsushita, N. Tsuchiya, K. Nakatsuka, T. Yanagitani, Precipitation and calcination process for yttrium aluminum garnet precursor powders synthesized by the urea method, J. Am. Ceram. Soc. 82 (8) (1999) 1977–1984.
[17] T. Takamori, L.D. David, Controlled nucleation for hydrothermal growth of yttrium aluminum garnet powders, J. Am. Ceram. Soc. 65 (9) (1986) 1282–1286.
[18] Y. Hakuta, T. Haganuma, K. Sue, T. Adschiri, K. Arai, Continuous production of phosphor YAG:Tb nanoparticles by hydrothermal synthesis in supercritical water, Mater. Res. Bull. 38 (2003) 1257–1265.
[19] M. Inoue, H. Otsu, H. Kominami, T. Inui, Synthesis of yttrium aluminum garnet by the glycothermal method, J. Am. Ceram. Soc. 74 (6) (1991) 1452–1454.
[20] M. Nyman, J. Caruso, M.J. Hampden-Smith, T.T. Kodas, Comparison of solid-state and spray-pyrolysis of yttrium aluminate powders, J. Am. Ceram. Soc. 80 (5) (1997) 1231–1238.
[21] Y.C. Kang, I.W. Lenggoro, S.B. Park, K. Okuyama, YAG:Ce phosphor particles prepared by ultrasonic spray pyrolysis, Mater. Res. Bull. 35 (2000) 789–798.
[22] K.T. Pillar, R.V. Kamat, V.N. Vaigya, D.D. Sood, Synthesis of yttrium aluminum garnet by the glycerol route, Mater. Chem. Phys. 44 (1996) 255–260.
[23] S. Shi, J. Wang, Combustion synthesis of Eu^{3+} activated $Y_3Al_5O_{12}$ phosphor nanoparticles, J. Alloys Compd. 327 (2001) 82–86.
[24] B.H. King, J.W. Halloran, Polycrystalline yttrium aluminum garnet fibers from colloidal sols, J. Am. Ceram. Soc. 7 (8) (1995) 2141–2148.
[25] V. Veith, S. Mathur, A. Kareiva, M. Jilavi, M. Zimmer, V. Huch, Low temperature synthesis of nanocrystalline $Y_3Al_5O_{12}$ (YAG) and Ce-doped YAG via different sol–gel methods, J. Mater. Chem. 9 (1999) 3069–3079.
[26] F.G. Qiu, X.P. Pu, J. Li, X.J. Liu, Y.B. Pan, J.K. Guo, Thermal behavior of the YAG precursor prepared by sol–gel combustion process, Ceram. Int. 31 (2005) 663–665.
[27] J. Li, Y.B. Pan, F.G. Qiu, Y.S. Wu, W.B. Liu, J.K. Guo, Synthesis of nanosized Nd:YAG powders via gel combustion, Ceram. Int. 33 (2007) 1047–1052.
[28] S.R. Jain, K.C. Adiga, V.R. Pai Verneker, A new approach to thermochemical calculations of condensed fuel-oxidizer mixtures, Combust. Flame 40 (1981) 71–79.
[29] S.S. Manoharan, K.C. Patil, Combustion synthesis of metal chromite powders, J. Am. Ceram. Soc. 75 (4) (1992) 1012–1015.
[30] S. Roy, W. Sigmund, F. Aldinger, Nanostructured yttria powders via gel combustion, J. Mater. Res. 14 (4) (1999) 1524–1531.
[31] S. Roy, A. Das Sharma, S.N. Roy, H.S. Maiti, Synthesis of $YBa_2Cu_3O_{7-x}$ powder by autoignition of citrate–nitrate gel, J. Mater. Res. 8 (11) (1993) 2761–2766.
[32] A. Chakrabort, P.S. Devi, S. Roy, H.S. Maiti, Low-temperature synthesis of ultrafine $La_{0.84}Sr_{0.16}MnO_3$ powder by an autoignition process, J. Mater. Res. 9 (4) (1994) 986–991.
[33] S. Ramanthan, M.B. Kakade, S.K. Roy, K.K. Kutty, Processing and characterization of combustion synthesized YAG powders, Ceram. Int. 29 (2003) 477–484.
[34] L.R. Pederson, G.D. Maupin, W.J. Weber, D.J. McReady, R.W. Stephens, Combustion synthesis of $YBa_2Cu_3O_{7-x}$: glycine/metal nitrate method, Mater. Lett. 10 (9/10) (1991) 437–443.
[35] M.K. Cinbulk, Effect of precursors and dopants on the synthesis and grain growth of calcium hexaluminate, J. Am. Ceram. Soc. 81 (12) (1998) 3157–3168.
[36] M.K. Cinbulk, Synthesis of yttrium aluminum garnet from a mixed-metal citrate precursor, J. Am. Ceram. Soc. 83 (5) (2000) 1276–1278.
[37] Y. Liu, Z.F. Zhang, J. Halloran, R.M. Laine, Yttrium aluminum garnet fibers from metalloorganic precursors, J. Am. Ceram. Soc. 81 (3) (1998) 629–645.
[38] M.A. Gülgün, O.O. Popoola, W.M. Kriven, Chemical synthesis and characterization of calcium aluminate powders, J. Am. Ceram. Soc. 77 (2) (1994) 531–539.
[39] J.G. Li, T. Ikegami, J.H. Lee, T. Mori, Low-temperature fabrication of transparent YAG ceramics without additives, J. Am. Ceram. Soc. 83 (4) (2000) 961–963.
[40] K.R. Han, H.J. Koo, C.S. Lim, A simple way to synthesize yttrium aluminum garnet by dissolving yttria powder in alumina sol, J. Am. Ceram. Soc. 82 (6) (1999) 1598–1600.
[41] X.Z. Guo, P.S. Devi, B.G. Ravi, J.B. Parise, S. Sampath, J.C. Hanson, Phase evolution of yttrium aluminum garnet (YAG) in a citrate–nitrate gel combustion process, J. Mater. Chem. 14 (2004) 1288–1292.
[42] C.K. Ullal, K.R. Balasubramaniam, A.S. Gandhi, V. Jayaram, Non-equilibrium phase synthesis in Al_2O_3–Y_2O_3 by spray pyrolysis of nitrate precursors, Acta Mater. 49 (2001) 2691–2699.
[43] Q.M. Lu, W.S. Dong, H.J. Wang, X.K. Wang, A novel way to synthesize yttrium aluminum garnet from metal-inorganic precursor, J. Am. Ceram. Soc. 85 (2) (2002) 490–492.